# PCCP



**View Article Online PAPER** 



Cite this: Phys. Chem. Chem. Phys., 2024, 26, 5597

# An effective method in modulating thermally activated delayed fluorescence (TADF) emitters from green to blue emission: the role of the phenyl ring†

Lijuan Wang, D Zhonggi Ge, Lin Xu and Yan Song \*\*D\*\*

Developing efficient blue emitters with high performance and low cost is crucial for the further development of organic light-emitting diodes (OLEDs). Based on the two experimentally reported green thermally activated delayed fluorescence (TADF) emitters, which are thioxanthone derivatives consisting of carbazole as an electron donor and 9H-thioxanthen-9-one-S,S-dioxide (SOXO) as an electron acceptor with donor-acceptor (D-A) or donor-acceptor-donor (D-A-D) structures, two new blue TADF emitters are designed by simply inserting a phenyl ring between D and A units. The TADF processes of the four thioxanthone derivatives are studied systematically through first-principles calculations. The role of the introduced phenyl ring in the excited state properties of the designed molecules is explored by analyzing the changes in molecular geometries, frontier molecular orbital distributions, the lowest singlet-triplet energy splitting ( $\Delta E_{ST}$ ), the spin orbit coupling (SOC) constants, the radiative decay rates  $(k_r)$  and the nonradiative decay rates  $(k_{nr})$ , as well as the intersystem crossing rates  $(k_{ISC})$  and reverse intersystem crossing rates  $(k_{RISC})$ . The results show that when incorporating phenyl units into the D-A and D-A-D structures, both high  $k_r$  and enhanced  $k_{RISC}$  are achieved in Cz-Ph-SOXO and DCz-DPh-SOXO, demonstrating that incorporating the phenyl unit in D-A and D-A-D structures is an efficient way for developing new SOXO-based TADF molecules. It is worth noting that the  $k_{RISC}$  values for Cz-Ph-SOXO and DCz-DPh-SOXO are significantly increased with respect to those of the experimental molecules. The present results would provide helpful guidelines for developing new SOXO-based TADF molecules experimentally.

Received 20th November 2023, Accepted 16th January 2024

DOI: 10.1039/d3cp05632e

rsc.li/pccp

## 1. Introduction

As the third generation of organic light emitting diode (OLED) emitters, thermally activated delayed fluorescence (TADF) materials, which can harvest both the singlet and triplet excitons through the efficient reverse intersystem crossing (RISC) process, have drawn more and more attention in recent years. 1-3 Unlike the conventional fluorescent and phosphorescent materials, the TADF emitters can utilize all the singlet and triplet excitons and realize high efficiency without the assistance of noble metals. Thus, there is a high potentiality to develop lower cost, but more promising OLED devices based on this class of materials. For an efficient TADF emitter, two key parameters, a small singlet-triplet energy splitting ( $\Delta E_{ST}$ ) and high photoluminescence quantum yield ( $\Phi_{PL}$ ), are requisite.<sup>4-7</sup>

School of Materials Science and Engineering, Harbin Institute of Technology at Weihai, 2 West Wenhua Road, Weihai, 264209, China. E-mail: sy@hitwh.edu.cn † Electronic supplementary information (ESI) available. See DOI: https://doi.org/ 10.1039/d3cp05632e

To achieve a small  $\Delta E_{ST}$ , the spatial separation of the highest occupied molecular orbital (HOMO) and the lowest unoccupied molecular orbital (LUMO) of the molecules are required and thereby the exchange integral (1) will be reduced based on the equation

$$\Delta E_{\text{ST}} = 2J = 2 \iint \phi_{\text{L}}(1) \phi_{\text{H}}(2) \left(\frac{e^2}{r_1 - r_2}\right) \phi_{\text{L}}(2) \phi_{\text{H}}(1) dr_1 dr_2.^{8,9} \text{ How-}$$

ever, the demand of the separated distribution of the HOMO/LUMO for a narrow  $\Delta E_{\rm ST}$  can suppress the transition dipole moment between the ground state (S<sub>0</sub>) and the first singlet excited state  $(S_1)$ , leading to a small oscillator strength (f) and low  $\Phi_{PL}$ . Therefore, the delicate balance between the spatial separation of the HOMO-LUMO wave function and the large f could be a compromise design strategy for efficient TADF emitters.4-7 So far, versatile molecular systems with TADF properties have been developed, including spiro-acidine, 10 triazine, 11 spirobifluorene,<sup>12</sup> phthalonitrile,<sup>13</sup> triptycene,<sup>8</sup> diphenyl sulfone derivatives, 14-17 and so on. Highly efficient sky-blue OLEDs with 37% external quantum efficiency have been achieved, which can be comparable to the excellent performance of phosphorescent OLEDs. 18 Despite significant Paper

progress having been made in recent years, developing highly efficient new TADF emitters with both small  $\Delta E_{\rm ST}$  and high  $\Phi_{\rm PL}$ is still a great challenge. The traditional design strategy for TADF emitters is combining an electron donor (D) and an electron acceptor (A) unit to spatially separate the HOMOs and LUMOs. 19,20 Generally, a phenyl linker is demanded to increase the D-A spatial separation distance and relieve the twisted angle between the D and the A.21,22 Compared with the D-Atype TADF emitters, D-A-D-type TADF emitters can facilitate a stronger intramolecular charge transfer and therefore smaller  $\Delta E_{\rm ST}$ , which can promote the highly efficient RISC progress and achieve excellent OLED performance. 23-31

Thioxanthone (TXO) and 9-H-thioxanthen-9-one-10,10dioxide (SOXO) units are excellent acceptor units for constructing highly efficient TADF materials. The  $\Delta E_{ST}$  of SOXO is reported to be lower than 0.3 eV, 32,33 and the SOXO core contains a ketone moiety which is alone able to produce delayed fluorescence.34,35 Several kinds of SOXO systems have been reported to exhibit excellent TADF properties. In 2014, Wang and co-workers reported two efficient TADF emitters of SOXO based derivatives with the D-A structure, using SOXO as the electron acceptor unit, and triphenylamine (TPA)/N-phenylcarbazole (PhCz) as the electron donor unit.36 Later on, they demonstrated a remarkable divergence in the photophysical properties of the SOXO based TADF emitters with different substitution positions of the PhCz donor.<sup>37</sup> In 2019, they designed four D-A-D region isomers with TADF properties by connecting two PhCz as donors at the different substituted positions of the phenyl group in the SOXO unit, highlighting the beneficial role of the different substituted positions of the acceptor unit in facilitating the adjustment of  $\Delta E_{\rm ST}$  and  $f^{38}$  In 2016, Su et al. investigated the structureperformance relationship of thioxanthone-based TADF emitters with substituted carbazole donors and inferior OLED performance was achieved for the symmetric D-A-D molecules with 2,7-substitutions.<sup>27</sup> Interestingly, in the same year, they reported blue and yellow TXO-based TADF emitters with the D-A-D structure with an external quantum efficiency (EQE) of over 20%, in which they introduced two triphenylamine (TPA) donor units at the 3 and 6 position of the TX (9-H-thioxanthen-9-one) unit. Ultrahigh EQE values of 23.7% and 24.3% are achieved for the symmetrical blue emitter 3,6-2TPA-TX and the yellow emitter 3,6-2TPA-TXO, respectively.<sup>39</sup> Although the SOXO-based TADF emitters have achieved excellent performance in OLED devices, the electroluminescence mechanism of this kind of material is still unclear. For the singlet-harvesting mechanism, both the singlet and triplet excited states are involved in the emission process, and the overall emission behavior relates to the individual properties of these states,  $\Delta E_{ST}$ , f, the spin orbit coupling (SOC) and the related intersystem crossing (ISC) and RISC processes. All of these properties should be considered sufficiently when engineering the chemical structures of the TADF emitters. 9,40,41 Therefore, a detailed understanding of the structural-property relationship of the organic TADF emitters is crucial for effective materials engineering, which facilitates the development of new efficient TADF emitters and promotes their applications in OLEDs.

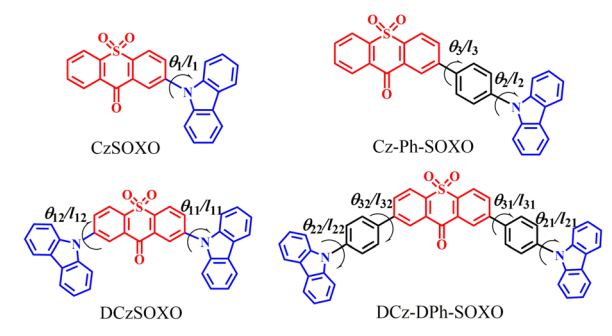


Fig. 1 Chemical structures of the studied thioxanthone-based molecules with D-A (CzSOXO), D- $\pi$ -A (Cz-Ph-SOXO), D-A-D (DCzSOXO) and D- $\pi$ -A- $\pi$ -D (**DCz-DPh-SOXO**) structures,  $\theta$  and l denote the main dihedral angles and bond lengths.

In this work, the electroluminescence mechanisms of two experimentally reported D-A and D-A-D type SOXO based TADF emitters (the chemical structures are plotted in Fig. 1) are systematically investigated using density functional theory (DFT) and time-dependent density functional theory (TD-DFT). Two new SOXO derivatives are designed via simply introducing the phenyl ring between donor and acceptor units with D- $\pi$ -A and D- $\pi$ -A- $\pi$ -D structures to further establish the structureproperty relationship. The influence of the phenyl ring on the excited state properties of the SOXO-based molecules is investigated. The photophysical properties, the radiative and nonradiative decay rates, the ISC and RISC rates, as well as SOC constants of the investigated molecules, are explored in detail. It was found that the TADF emitters are modulated from green to blue emission, and the radiative decay rates and the rates of the RISC process are also enhanced through simply incorporating phenyl rings into the experimental molecules.

## Theoretical methods

The decay rate constants from the S<sub>1</sub> to S<sub>0</sub> states and the interconversion rate constants between the S<sub>1</sub> and T<sub>1</sub> states are key parameters in determining the electroluminescence mechanism of the SOXO-based TADF molecules. The radiative decay rate  $k_r$  is calculated by the Einstein spontaneous emission equation as follows:42-44

$$k_{\rm r} = \frac{f\Delta E_{\rm fi}^2}{1.499} \tag{1}$$

where f is the oscillator strength and  $\Delta E_{\rm fi}$  is the vertical emission energy with the unit of wavenumber  $(cm^{-1})$ .

The nonradiative decay rate  $k_{\rm nr}$  can be obtained based on Fermi's golden rule and the first-order perturbation theory 45,46

$$k_{\rm nr} = \frac{2\pi}{\hbar^2} \sum_{\rm u.v} P_{\rm iv} |\hat{H}_{\rm fu,iv}|^2 \delta(E_{\rm iv} - E_{\rm fu})$$
 (2)

Here, the delta function  $\delta$  is to ensure the conservation of energy;  $P_{iv}$  is the Boltzmann distribution function for the initial vibronic manifold;  $\hat{H}_{\text{fu,iv}}$  is the interaction operator between two different Born-Oppenheimer states, consisting of two

**PCCP Paper** 

contributions as below46

$$\hat{H}\Psi_{iv} = \hat{H}^{BO}\Phi_{i}(r,Q)\Theta_{iv}(Q) + \hat{H}^{SO}\Phi_{i}(r,Q)\Theta_{iv}(Q)$$
 (3)

here,  $\hat{H}^{BO}$  is the nonadiabatic coupling and  $\hat{H}^{SO}$  is the spinorbit coupling, r and Q are the electronic and normal mode coordinates.  $\Phi_i$  is the electron wave function, and  $\Theta_{iv}$  is the nuclear vibrational wave function.

The internal conversion rate constant between two electronic states with the same spin multiplicity can be evaluated by using the first-order perturbation theory as<sup>45</sup>

$$k_{\rm IC} = \frac{1}{\hbar^2} R_{kl} \int_{-\infty}^{\infty} \mathrm{d}t \, \mathrm{e}^{\mathrm{i}\omega_{\rm if}t} \rho_{\rm fi}^{\rm ic}(t,T) \tag{4}$$

Here, the nonadiabatic electronic coupling matrix element  $R_{
m kl} = \left\langle \Phi_{
m f} \middle| \hat{P}_{
m fk} \middle| \Phi_{
m i} \right\rangle \left\langle \Phi_{
m i} \middle| \hat{P}_{
m fl} \middle| \Phi_{
m f} \right\rangle, \quad \hat{P}_{
m fk} = -i\hbar rac{\partial}{\partial O_{
m fk}} \quad {
m is} \quad {
m the} \quad {
m normal}$ momentum operator of the  $k_{\rm th}$  normal mode in the final electronic states.  $\Phi_{\rm f}$  and  $\Phi_{\rm i}$  are the wavefunctions of the final state and the initial states, respectively.  $\rho_{\rm fi}^{\rm ic}$  is the thermal vibration correlation function (TVCF), ^{42-44} which is  $Z_i^{-1} \operatorname{Tr} \left[ \hat{P}_{fk} \mathrm{e}^{-\mathrm{i}\tau_f \hat{H}_f} \hat{P}_{fl} \mathrm{e}^{-\mathrm{i}\tau_i \hat{H}_i} \right]$ . Here,  $Z_i$  represents the partition function.

The intersystem crossing rate constant between the singlet and triplet states can be evaluated based on the following equation:42,43

$$k_{\rm ISC} = \frac{1}{\hbar} \langle \Phi_{\rm f} | \hat{H}^{\rm SO} | \Phi_{\rm i} \rangle \int_{-\infty}^{\infty} \mathrm{d}t \left[ \mathrm{e}^{\mathrm{i}\omega_{\rm if}t} Z_i^{-1} \rho_{\rm ISC}(t,T) \right] \tag{5}$$

The detailed derivation of these equations can be found in Peng and Shuai's work.45-47

# 3. Computational details

The geometric optimizations and frequency calculations of the So states are performed via density functional theory (DFT), while the excited singlet and triplet states are optimized through the time-dependent DFT (TD-DFT) approach. Since the excited state properties of TADF molecules with charge transfer character are functional dependent, several exchangecorrelation functionals, including B3LYP, 48 PBE0, 49 PBE0-1/3, 50 BMK<sup>51</sup> and M062X<sup>52</sup> with different HF exchange percentages in the XC functional of 20%, 25%, 33.33%, 42% and 54%, and two range-separated hybrid functionals, CAM-B3LYP<sup>53</sup> and ωB97XD,<sup>54</sup> are used to calculate the absorption and emission wavelengths of CzSOXO and DCzSOXO combining with the 6-31G(d)<sup>55-57</sup> basis set (see Table 1). It was shown that the results based on the PBE0-1/3 functional agree well with the experimental values. The PBE0-1/3 functional and 6-31G(d) basis sets are therefore used to evaluate the ground and excited state properties of the studied molecules. All calculations are performed in a toluene solvent with the Polarizable Continuum Model (PCM)<sup>58</sup> using the Gaussian 09 software package.<sup>59</sup>

Based on the electronic properties, the calculations of the radiative and nonradiative decay rates, as well as the intersystem crossing rate and reverse intersystem crossing rate constants are finished through the Molecular Material Property

**Table 1** The calculated absorption  $(\lambda_{ab})$  and emission  $(\lambda_{em})$  wavelengths of CzSOXO and DCzSOXO based on different functionals, together with the experimental values for comparison

	CzSOXO		DCzSOXO		
	$\lambda_{ab}$ (nm)	$\lambda_{ab} (nm)$ $\lambda_{em} (nm)$		$\lambda_{\mathrm{em}}$ (nm)	
B3LYP	521	700	543	730	
PBE0	478	617	498	642	
PBE0-1/3	423	524	440	542	
BMK	393	474	408	476	
M062X	361	421	372	425	
CAM-B3LYP	352	411	364	415	
ωB97XD	341	389	349	395	
Expt. <sup>26</sup>	404	536	406	546	

Prediction Package (MOMAP).60-65 The SOC matrix elements are computed from the quadratic response function by the Dalton program package. 66,67

In addition, to characterize the geometric changes between the S<sub>0</sub> and S<sub>1</sub> states and between the S<sub>1</sub> and T<sub>1</sub> states, the root of the mean of squared displacement (RMSD) is calculated using the following equation:

RMSD = 
$$\sqrt{\frac{1}{N}} \sum_{i}^{\text{natom}} \left[ (x_i - x_i')^2 + (y_i - y_i')^2 + (z_i + z_i')^2 \right]$$
 (6)

where i is the atomic ordinal number. To analyze the excitation properties of the investigated molecules, the electron-hole (e-h) distributions and the overlaps of e-h of the S<sub>1</sub> states are calculated through the Multiwfn<sup>68,69</sup> software.

### Results and discussions

#### Molecular geometric structures

The molecular geometric structures play a crucial role in determining both the electronic structures and photophysical properties. A large distorted dihedral angle between D and A units generally allows efficient spatial separation of the HOMO and the LUMO to achieve a small  $\Delta E_{\rm ST}$  value. The geometric structures of the So, S1 and excited triplet states for all the investigated molecules are optimized based on the PBE0-1/3/6-31G(d) level in a toluene solvent. The main dihedral angles and bond lengths (as shown in Fig. 1) of CzSOXO, DCzSOXO, Cz-Ph-**SOXO** and **DCz-DPh-SOXO** based on the optimized  $S_0$ ,  $S_1$  and  $T_1$ geometries in toluene are listed in Table 2. It can be seen that the molecular geometries between the S<sub>0</sub> and S<sub>1</sub> states are significantly altered when changing the molecular types. In the  $S_0$  states, the dihedral angle  $(\theta_1)$  between D and A moieties of CzSOXO is 50°, which is almost the same as that of DCzSOXO. However, when inserting the phenyl rings between the D and A unit in CzSOXO and DCzSOXO, the dihedral angles between the SOXO group and the phenyl ring are decreased to 37° for Cz-Ph-SOXO and DCz-DPh-SOXO, respectively. The corresponding bond lengths  $(l_1)$  are also 0.08 Å larger than those of CzSOXO and DCzSOXO. When comparing the dihedral angles in Table 2 between the So and S1 states, it can be found that the dihedral angles between D and A units are increased by around 14° for CzSOXO and DCzSOXO. While the largest

Table 2 The main dihedral angles (in degree) and bond lengths (in angstrom) of the designed SOXO-based molecules based on the optimized  $S_0$  and  $S_1$  geometries in toluene

Molecules	Bond parameters	S <sub>0</sub> geometry	S <sub>1</sub> geometry	T <sub>1</sub> geometry
CzSOXO	$\theta_1$	50	64	42
	$l_1$	1.40	1.43	1.38
DCzSOXO	$ heta_{11}/ heta_{12}$	49/49	64/53	49/43
	$l_{11}/l_{12}$	1.40/1.40	1.43/1.41	1.40/1.38
Cz-Ph-SOXO	$ heta_3/ heta_2$	37/54	33/48	46/2
	$l_3/l_2$	1.48/1.41	1.47/1.40	1.41/1.39
DCz-DPh-SOXO	$\theta_{31}/\theta_{32}/\theta_{21}/\theta_{22}$	36/37/53/126	35/33/56/132	4/36/46/126
	$l_{31}/l_{32}/l_{21}/l_{22}$	1.48/1.48/1.41/1.41	1.48/1.47/1.41/1.40	1.41/1.48/1.39/1.41

dihedral angle deviations between the  $S_0$  and  $S_1$  states for Cz-Ph-SOXO and DCz-DPh-SOXO have occurred between the carbazole unit and the inserted phenyl ring, and the value at  $S_1$  states is decreased by  $6^\circ$  with respect to those of  $S_0$  states. The decreased dihedral angles at  $S_0$  and  $S_1$  states make the geometries of Cz-Ph-SOXO and DCz-DPh-SOXO become more planar compared with those of CzSOXO and DCzSOXO. It can also be found that the  $T_1$  geometries of the studied molecules change significantly compared with the  $S_1$  geometries, and the selected dihedral angles of Cz-Ph-SOXO and DCz-DPh-SOXO at the  $T_1$  state show greater changes than those of CzSOXO and DCzSOXO with respect to those at the  $S_1$  state.

To quantitatively characterize the geometry changes between S<sub>0</sub> and S<sub>1</sub> states and between S<sub>1</sub> and T<sub>1</sub> states, the RMSD analysis of the investigated molecules is performed and the results are presented in Fig. 2. It can be found that the RMSD values between So and St states for CzSOXO and DCzSOXO are 0.344 and 0.394 Å, respectively. When bringing the phenyl ring between D and A units, the RMSD values decrease to 0.118 and 0.122 Å, respectively. The geometric changes between S<sub>1</sub> and T<sub>1</sub> states show much larger RMSD values than those between S<sub>0</sub> and S<sub>1</sub> states. The large geometry changes will lead to large reorganization energy between the corresponding two states and consequently lead to larger nonradiative decay rates. The geometry changes of the ground state and the excited states via changing the molecular types will definitely affect the distributions of the frontier molecular orbitals and the photophysical properties as discussed below.

#### 4.2 Frontier molecular orbitals

The distributions of the frontier molecular orbitals play an important role in determining  $\Delta E_{ST}$ , which is closely related to the steric hindrance of the molecular geometry. The more separated distributions between HOMOs and LUMOs, the smaller  $\Delta E_{\rm ST}$  will be. On the other hand, the spatial overlap between HOMO and LUMO is essential to achieve high radiative decay rates  $(k_r)$ . The distributions and energy levels of HOMOs and LUMOs for the investigated molecules in the So state are plotted in Fig. 3. It can be clearly seen that the HOMOs of CzSOXO and DCzSOXO are predominantly located on the donor units, and partially on the acceptor groups, and the LUMOs are mainly distributed on the acceptor moieties, and a small portion is distributed on the donor unit, ensuring a partial overlap between the distributions of HOMOs and LUMOs. When inserting the phenyl ring between D and A groups, smaller overlaps between HOMOs and LUMOs for Cz-Ph-SOXO and DCz-DPh-SOXO can also be found, which facilitates obtaining small  $\Delta E_{ST}$ . It can also be found that the energy gaps between HOMOs and LUMOs for Cz-Ph-SOXO and DCz-DPh-SOXO are decreased by 0.14 and 0.10 eV compared with CzSOXO and DCzSOXO, respectively.

To analyze the excitation properties and quantitatively predict the degree of overlap between HOMOs and LUMOs, the electron-hole (e-h) distribution and overlap of e-h for the  $S_1$  state of the investigated molecules are provided in Fig. 4. It can be seen that there are obvious overlaps of e-h for **CzSOXO** and **DCzSOXO**, mainly occurring on the acceptor unit. For the designed molecules **Cz-Ph-SOXO** and **DCz-DPh-SOXO**, the e-h

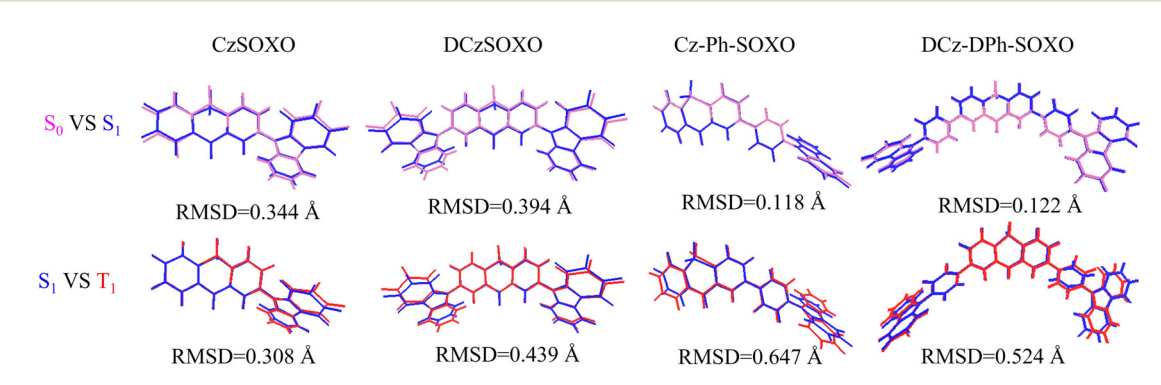


Fig. 2 Comparison of the geometries between  $S_0$  (pink),  $S_1$  (blue) and  $T_1$  (red) states in toluene for investigated molecules (RMSD values are presented).

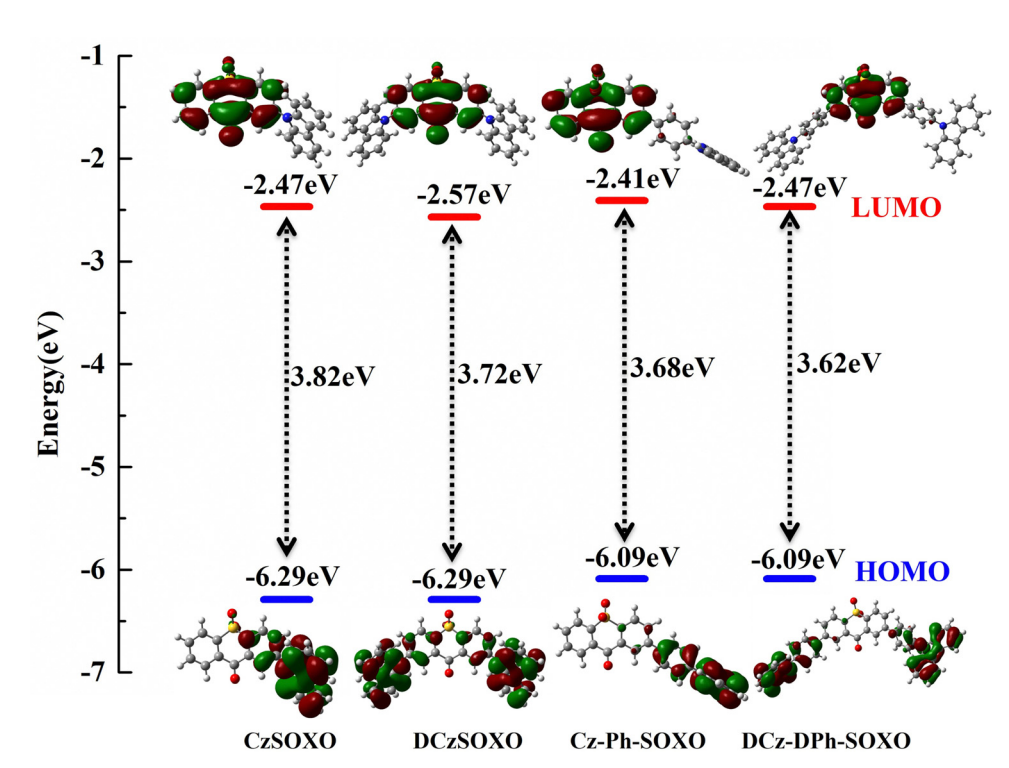


Fig. 3 The distributions and energy levels of the frontier molecular orbitals for the studied molecules at the  $S_0$  state (isovalue is 0.02).

overlap became smaller than those of CzSOXO and DCzSOXO, indicating that they may possess smaller  $\Delta E_{\rm ST}$ . It can also be

noticed that the e-h distributions are separated significantly for all the investigated molecules, indicating that the charge

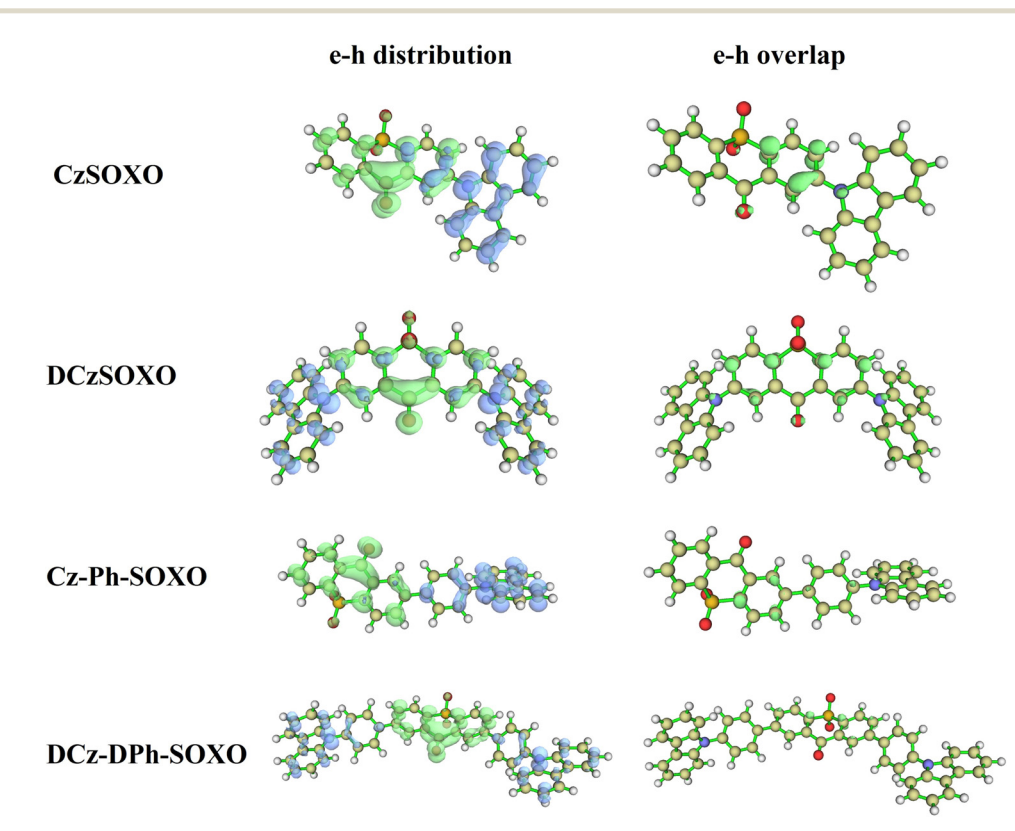


Fig. 4 The electron-hole (e-h) distributions and overlaps of e-h for the S1 states of CzSOXO, DCzSOXO, Cz-Ph-SOXO and DCz-DPh-SOXO (isosurface value is 0.002).

Paper

**Table 3** The  $S_r$ , D, t, H, and  $\Delta r$  index of the investigated molecules between

Molecules	S <sub>r</sub> /a.u.	D/Å	t/Å	H/Å	$\Delta r_{\mathrm{S_1}}/\mathrm{\mathring{A}}$	$\Delta r_{\mathrm{S}_2}$ /Å
CzSOXO	0.32	5.08	4.62	2.81	5.66	6.49
DCzSOXO	0.38	1.44	0.08	4.40	1.58	1.62
Cz-Ph-SOXO	0.24	8.75	6.26	3.15	9.50	4.45
DCz-DPh-SOXO	0.29	3.52	1.78	6.02	4.88	4.94

transfer process can occur in all the molecules. To further analyze the inside mechanisms, the spatial separation of holes and electrons  $S_r$ , the charge transfer (CT) length D, the degree of separation of holes and electrons t, the reflection of the overall average distribution breadth of electrons and holes H, and the  $\Delta r$  index for the  $S_1$  and  $S_2$  states used to measure the charge transfer length during the electron excitation, are calculated via Multiwfn software<sup>68</sup> and the results are listed in Table 3. The calculated parameters in Table 3 also verify the above findings. When the t index is larger than zero, this implies that the distributions of holes and electrons are effectively separated because of the CT process. The  $\Delta r$  index for the S<sub>1</sub> and S<sub>2</sub> states is used to measure the charge transfer length during the electron excitation, and the larger the  $\Delta r$  value is, the more likely the excitation is a CT mode. It can be found that the  $S_r$  index of CzSOXO (0.32) and DCzSOXO (0.38) is larger than Cz-Ph-SOXO (0.24) and DCz-DPh-SOXO (0.29), indicating the larger overlap between holes and electrons, which is in accord with the e-h distributions as discussed above. It can also be found that t indices are all greater than zero, suggesting that sufficient hole and electron separations occurred in these molecules due to the CT process. However, the t index of **DCzSOXO** is as small as 0.08, demonstrating that there is some overlap between the hole and the electron. For the S<sub>1</sub> and S<sub>2</sub> states,  $\Delta r$  of all the molecules is larger than the threshold distinguishing the local excited (LE) state and the CT excited states of 2 Å, except that of DCzSOXO, indicating that they are LE states. It is also illustrated in Table 3 that the e-h overlaps can be decreased when incorporating the phenyl ring in Cz-Ph-SOXO and DCz-DPh-SOXO with respect to those of CzSOXO and DCzSOXO.

#### 4.3 $\Delta E_{ST}$ and transition properties

The singlet-triplet energy gap ( $\Delta E_{ST}$ ) for TADF molecules is one of the key parameters for the RISC process, which is correlated to the distributions of the HOMO and the LUMO. The excitation energies of  $S_1$  and  $T_1$  states based on the  $S_0$ ,  $S_1$  and  $T_1$  geometries and the vertical and adiabatic energy splitting

between the  $S_1$  and  $T_1$  states for the investigated molecules are provided in Table 4. It can be noticed that the adiabatic energy gaps between the  $S_1$  and  $T_1$  states for **CzSOXO** and **DCzSOXO** are 0.35 and 0.31 eV, respectively. When inserting the phenyl ring between D and A units in **CzSOXO** and **DCzSOXO**, these values are increased to 0.63 and 0.59 eV, respectively. The results are in agreement with the analysis of the geometric changes. However, the energy gap of **Cz-Ph-SOXO** between the  $T_3$  and  $S_1$  states is much smaller than that of **CzSOXO** between  $T_1$  ( $T_2$ ) and  $S_1$  states (see Fig. 5), demonstrating that the ISC and the RISC processes may occur from the  $S_1$  to  $T_3$  states for **Cz-Ph-SOXO**. Similarly, for **DCzSOXO** and **DCz-DPh-SOXO**, the nearest triplet states to the  $S_1$  state are  $T_2$  ( $T_3$ ) and  $T_3$  ( $T_4$ ) states, respectively. So, the ISC process may occur from  $S_1$  to  $T_2$  ( $T_3$ ) and  $T_3$  ( $T_4$ ) states, respectively.

The transition properties of excited states are also vital in determining the excited state properties. The natural transition orbital (NTO) analyses of the  $S_1$  and  $T_1$  states in toluene are performed for the investigated molecules. As shown in Fig. S1–S4 (ESI†), the highest occupied natural transition orbital (hole) and the lowest unoccupied natural transition orbital (particle) predominate the transition for  $S_1$  and  $T_1$  states. The  $S_1$  states of the studied molecules generally exhibit charge transfer (CT) characters. For the  $T_1$  and higher triplet states ( $T_2$ ,  $T_3$  or  $T_4$  states), it can be found that all the molecules not only show significant local excited (LE) properties, but also partial CT characters. The CT characters can help to achieve larger  $k_{\rm RISC}$ , therefore realizing a more efficient RISC process. <sup>22</sup>

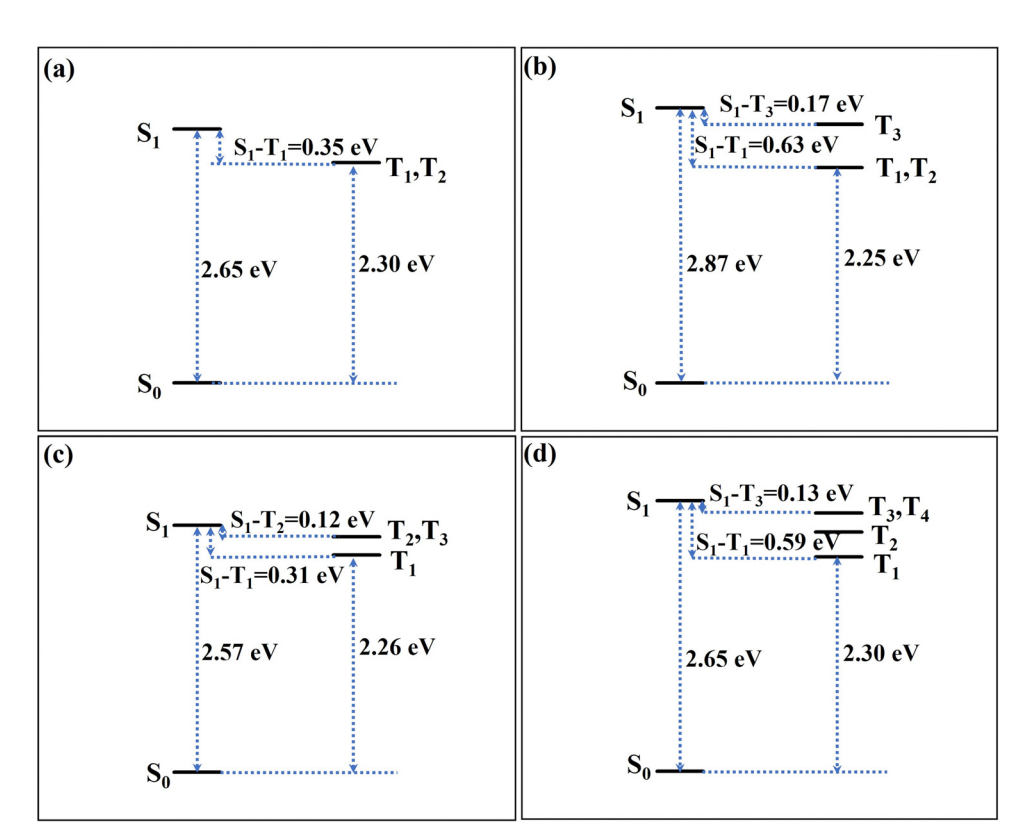
#### 4.4 Photophysical property

The photophysical property is vital in exploring the TADF process of the investigated molecules. The absorption and emission wavelength as well as the oscillator strength of the S<sub>1</sub> state in a toluene solvent are provided in Table 5, together with the available experimental data. It can be found that the deviation between the theoretical and experimental absorption wavelengths of CzSOXO and DCzSOXO is less than 34 nm (with a relative difference of 7.7%). The calculated emission wavelengths are also in good agreement with the experimental results, and the deviations are within 12 nm. The emission wavelengths of CzSOXO and DCzSOXO are 524 and 542 nm, respectively, which are green emitters. While introducing the phenyl rings between the D and the A to CzSOXO and DCzSOXO make the emission wavelengths of Cz-Ph-SOXO and DCz-DPh-SOXO blue-shifted to 468 and 475 nm, respectively, which are blue emitters. When introducing the phenyl ring to CzSOXO

Table 4 The excitation energies of the  $S_1$  and  $T_1$  states based on  $S_0$  and  $S_1$  geometries and the energy difference between the  $S_1$  and  $T_1$  states for the investigated molecules (in unit of eV)

S <sub>0</sub> geor		<sub>0</sub> geometry		S <sub>1</sub> geometry		T <sub>1</sub> geometry		Adiabatic		
Molecules	$S_1$	$T_1$	$\Delta E_{\rm ST}$	$S_1$	$T_1$	$\Delta E_{\rm ST}$	$S_1$	$T_1$	$\Delta E_{\rm ST}$	$\Delta E_{ m ST}$
CzSOXO DCzSOXO Cz-Ph-SOXO DCz-DPh-SOXO	2.93 2.82 3.11 3.06	2.63 2.54 2.71 2.68	0.30 0.28 0.40 0.38	2.37 2.29 2.65 2.61	2.24 2.16 2.35 2.33	0.13 0.13 0.30 0.28	2.49 2.41 2.75 2.71	1.85 1.85 1.77 1.77	0.64 0.56 0.98 0.94	0.35 0.31 0.63 0.59

**PCCP** 



The energy landscape of the vertical excitation of CzSOXO (a), Cz-Ph-SOXO (b), DCzSOXO (c) and DCz-DPh-SOXO (d).

**Table 5** The calculated absorption ( $\lambda_{ab}$ ) and emission ( $\lambda_{em}$ ) wavelengths as well as the oscillator strength based on the PBE0-1/3/6-31G(d) level in a toluene solvent for the investigated molecules (the experimental values are also listed in the parentheses for comparison)

Molecules	$\lambda_{ab}$ (nm)	$f_{ m VA}$	$\lambda_{\mathrm{em}} \ (nm)$	$f_{ m VE}$
CzSOXO	423 (404 <sup>26</sup> )	0.0405	524 (536 <sup>26</sup> )	0.0145
DCzSOXO	440 (406 <sup>26</sup> )	0.0431	542 (546 <sup>26</sup> )	0.0157
Cz-Ph-SOXO	399	0.0613	468	0.0622
DCz-DPh-SOXO	405	0.0838	475	0.0665

and DCzSOXO between the D and A groups, the oscillator strengths of Cz-Ph-SOXO and DCz-DPh-SOXO are increased by 1.5 and 2 times, respectively, with respect to those of CzSOXO and DCzSOXO for the absorption process. While for the emission process, the oscillator strengths of Cz-Ph-SOXO and DCz-DPh-SOXO are also enhanced by 6 times than those of CzSOXO and DCzSOXO. From the perspective of oscillator strengths, it can be determined that the designed molecules (Cz-Ph-SOXO and DCz-DPh-SOXO) possess much better TADF properties compared with the experimental molecules (CzSOXO and DCzSOXO). Therefore, incorporating the phenyl ring between D and A moieties could be an efficient way for designing new efficient SOXO-based TADF molecules.

#### **Excited state dynamics** 4.5

For TADF emitters, the rate constants of radiative  $(k_r)$  and nonradiative  $(k_{nr})$  processes from the  $S_1$  to  $S_0$  state, as well as

the intersystem crossing  $(k_{\rm ISC})$  and reverse intersystem crossing  $(k_{RISC})$  rates play an important role in the dynamic process of the excited states. It is widely known that the ISC and RISC processes are related to not only the adiabatic energy gap between the S<sub>1</sub> and T<sub>1</sub> states, but also the SOC between the singlet and triplet states. The SOC constants between the S<sub>1</sub> and T<sub>1</sub> (T<sub>2</sub>, T<sub>3</sub> and T<sub>4</sub>) states are calculated based on the S<sub>1</sub> geometries through the Dalton66,67 package, as shown in Table 6. The  $k_r$  and  $k_{nr}$  from the  $S_1$  to  $S_0$  state as well as  $k_{ISC}$ and  $k_{RISC}$  between the S<sub>1</sub> and T<sub>1</sub> (T<sub>2</sub>, T<sub>3</sub> and T<sub>4</sub>) states in toluene are provided in Table 7. The radiative decay rates of CzSOXO and DCzSOXO are  $3.52 \times 10^6$  and  $3.56 \times 10^6$  s<sup>-1</sup>, respectively. While this value for Cz-Ph-SOXO and DCz-DPh-SOXO is increased to  $1.89 \times 10^7$  and  $1.96 \times 10^7$  s<sup>-1</sup>, respectively, which agrees with the values of oscillator strengths. However, the nonradiative decay rates  $(k_{nr})$  are all larger than the radiative rates  $(k_r)$  for **CzSOXO** and **DCzSOXO**, which is not beneficial for the light-emitting process. This is because the nonradiative

Table 6 The spin-orbit coupling (SOC) constants between the S<sub>1</sub> state and the selected triplet states in toluene for the investigated molecules (all the SOC values are in unit of cm<sup>-1</sup>)

Molecules	$\langle S_1  \mathcal{H}_{SO}  T_1\rangle$	$\langle S_1  \mathcal{H}_{SO}  T_2\rangle$	$\langle S_1 H_{SO} T_3\rangle$	$\langle S_1   H_{SO}   T_4 \rangle$
CzSOXO	0.228	0.358	_	_
DCzSOXO	0.215	0.183	0.366	_
Cz-Ph-SOXO	0.158	0.432	0.374	_
DCz-DPh-SOXO	0.141	0.158	0.043	0.365

**Table 7** The rate constants of radiative  $(k_r)$  and nonradiative  $(k_{nr})$  from the  $S_1$  to  $S_0$  state as well as the ISC  $(k_{ISC})$  and RISC  $(k_{RISC})$  between the  $S_1$  and  $T_1$   $(T_2, T_3)$  and  $T_4$  states in toluene (all the rates are in unit of  $s^{-1}$ )

Molecules	CzSOXO	DCzSOXO	Cz-Ph-SOXO	DCz-DPh-SOXO
$k_{\rm r} (S_1 \rightarrow S_0)$	$3.52 \times 10^{6}$	$3.56 \times 10^{6}$	$1.89 \times 10^{7}$	$1.96 \times 10^{7}$
$k_{\rm nr}\left(S_1 \to S_0\right)$	$5.14\times10^{10}$	$8.40 \times 10^{10}$	$7.50 \times 10^{5}$	$3.83 \times 10^{6}$
$k_{\rm ISC} (S_1 \rightarrow T_1)$	$8.27 \times 10^{6}$	$1.02\times10^6$	$7.00 \times 10^{4}$	$5.65  imes 10^4$
$k_{\text{RISC}} \left( \mathbf{T}_1 \to \mathbf{S}_1 \right)$	$9.89\times10^{0}$	$1.80\times10^{0}$	$6.58  imes 10^{-5}$	$1.82 \times 10^{-2}$
$k_{\rm ISC} \left( \mathbf{S}_1 \rightarrow \mathbf{T}_2 \right)$	$2.06\times10^{7}$	$2.53 \times 10^{6}$	$5.09  imes 10^5$	$1.59  imes 10^4$
$k_{\text{RISC}} \left( \mathbf{T}_2 \rightarrow \mathbf{S}_1 \right)$	$2.39 \times 10^{1}$	$6.82 \times 10^{2}$	$3.01 \times 10^{-4}$	$6.32 \times 10^{-5}$
$k_{\rm ISC} \left( \hat{\mathbf{S}}_1 \rightarrow \mathbf{T}_3 \right)$	_	$1.01\times10^7$	$5.56  imes 10^5$	$1.43 \times 10^{3}$
$k_{\text{RISC}} \left( \mathbf{T}_3 \rightarrow \mathbf{S}_1 \right)$	_	$2.92 \times 10^{3}$	$1.41 \times 10^{6}$	$2.66 \times 10^{4}$
$k_{\rm ISC} \left( S_1 \rightarrow T_4 \right)$	_	_	_	$1.02\times10^{5}$
$k_{\text{RISC}} \left( \mathbf{T}_4 \to \mathbf{S}_1 \right)$	_	_	_	$2.50 \times 10^{6}$

process is sensitive to the environment, and the calculated results are based on the single molecule model and without considering the intermolecular interaction. So when made into OLEDs, the nonradiative rates of the designed molecules can be reduced significantly than the calculated values as illustrated in previous studies.  $^{70-72}$  While  $k_{\rm nr}$  of Cz-Ph-SOXO and DCz-DPh-SOXO is significantly decreased compared with  $k_{\rm r}$ , which is beneficial for the light-emitting process. It is also found in Table 6 that the calculated SOC values between the  $S_1$  state and the triplet state closest to the  $S_1$  state are larger than those values between the  $S_1$  and other triplet states.

For CzSOXO, the  $T_1$  and  $T_2$  states are degenerate, and both the T<sub>1</sub> and T<sub>2</sub> states participate in the ISC and RISC processes. The  $k_{\rm ISC}$  (2.06 × 10<sup>7</sup> s<sup>-1</sup>) and  $k_{\rm RISC}$  (2.39 × 10<sup>1</sup> s<sup>-1</sup>) between the S<sub>1</sub> and T<sub>2</sub> states are more effective than those between the S<sub>1</sub> and T<sub>1</sub> states due to the larger SOC values between the S<sub>1</sub> and T<sub>2</sub> states. It can be seen in Table 7 that the  $T_1$ ,  $T_2$  and  $T_3$  states of DCzSOXO are all involved in the ISC and RISC processes. The most efficient route of the ISC and RISC processes for DCzSOXO is between the S<sub>1</sub> and T<sub>3</sub> states, and  $k_{\rm ISC}$  and  $k_{\rm RISC}$  are 1.01  $\times$  $10^7 \, \mathrm{s}^{-1}$  and  $2.92 \times 10^3 \, \mathrm{s}^{-1}$ , respectively. It can also be found in Fig. 5 that the T<sub>2</sub> and T<sub>3</sub> states of **DCzSOXO** are degenerate. However, the energy gap between  $T_1$  and  $T_2$  ( $T_3$ ) states is as small as 0.19 eV, so the internal conversion process will occur quickly from the  $T_2$  ( $T_3$ ) to the  $T_1$  state, and the RISC process might also happen from the T<sub>1</sub> to S<sub>1</sub> state. For Cz-Ph-SOXO and DCz-DPh-SOXO,  $k_{\rm ISC}$  values of the most effective route are decreased to  $5.56 \times 10^5$  and  $1.02 \times 10^5$  s<sup>-1</sup>, respectively. However,  $k_{RISC}$  values of Cz-Ph-SOXO (1.41  $\times$  10<sup>6</sup> s<sup>-1</sup>) and **DCz-DPh-SOXO**  $(2.50 \times 10^6 \text{ s}^{-1})$  of the most effective routes are significantly increased compared with those of CzSOXO  $(2.39 \times 10^{1} \text{ s}^{-1})$  and **DCzSOXO**  $(2.92 \times 10^{3} \text{ s}^{-1})$ , demonstrating that Cz-Ph-SOXO and DCz-DPh-SOXO are more facilitated to the occurrence of the RISC process. It can also be found that the RISC from the  $T_1$  ( $T_2$ ) to  $S_1$  state is very small for **Cz-Ph-SOXO**, which is due to the larger energy gap (0.46 eV) between the T<sub>3</sub> and  $T_1$  ( $T_2$ ) states. Therefore, the internal conversion process from the  $T_3$  to  $T_1$  ( $T_2$ ) state will be slow and the RISC process for Cz-Ph-SOXO mainly occurs from the  $T_3$  to  $S_1$  state. Similarly, for **DCz-DPh-SOXO**, the energy gap between  $T_3$  ( $T_4$ ) and  $T_1$  states is also as large as 0.46 eV, so the main ISC and RISC processes have happened between the  $S_1$  and  $T_3$  ( $T_4$ ) states.

In addition, the phosphorescence rates  $(k_{\rm p})$  from the  $\rm T_1$  to  $\rm S_0$  states calculated through MOMAP<sup>60–65</sup> software for all the investigated molecules are presented in Table S1 (ESI†). It can be found that the values of  $k_{\rm RISC}$  are apparently much larger than the corresponding  $k_{\rm p}$ , indicating that the reverse intersystem crossing process can successfully compete with the phosphorescence process. Based on the analysis of the dynamics of the excited states, it can be concluded that the designed molecules Cz-Ph-SOXO and DCz-DPh-SOXO with high  $k_{\rm r}$  and efficient  $k_{\rm RISC}$  can be used as excellent TADF emitters. Therefore, incorporating phenyl units into D–A and D–A–D type molecules is a good strategy for developing new efficient SOXO-based TADF emitters, and the emission color can also be modulated from green to blue simply by introducing the phenyl ring.

### 5. Conclusions

In summary, the photophysical processes and excited state dynamics of four SOXO-based molecules are investigated based on the first principles calculation. It is found that incorporating phenyl units between the donor and acceptor groups and changing the molecular types can significantly modulate the excited state properties of these molecules. The TADF mechanisms of the studied molecules are revealed by calculating  $k_r$ ,  $k_{nr}$ ,  $k_{ISC}$  and  $k_{RISC}$ ,  $\Delta E_{\rm ST}$  and SOC based on the thermal vibration correlation function method and TD-DFT approach. Results show that the emission wavelengths of Cz-Ph-SOXO and DCz-DPh-SOXO are also modulated from green to blue by simply inserting the phenyl ring between the donor and acceptor groups. For the designed molecules Cz-Ph-SOXO and DCz-DPh-SOXO, the  $k_r$  values increased significantly compared with those of CzSOXO and DCzSOXO. The  $k_{\rm ISC}$  values of Cz-Ph-SOXO and DCz-DPh-SOXO are relatively smaller than those of CzSOXO and DCzSOXO. However, the  $k_{RISC}$ values of Cz-Ph-SOXO and DCz-DPh-SOXO are significantly increased compared with those of CzSOXO and DCzSOXO, demonstrating that Cz-Ph-SOXO and DCz-DPh-SOXO are more facilitated to achieve the TADF process. In particular, the  $k_{RISC}$ values of Cz-Ph-SOXO and DCz-DPh-SOXO reached up to 1.41  $\times$  $10^6 \, \mathrm{s}^{-1}$  and  $2.50 \times 10^6 \, \mathrm{s}^{-1}$ , respectively, which is beneficial to the occurrence of delayed fluorescence. Our results would be helpful for developing new SOXO-based TADF materials experimentally.

**PCCP** Paper

## Conflicts of interest

The authors have no conflicts to disclose.

## Acknowledgements

This work was supported by the Natural Science Foundation of Shandong, China, Grant No. ZR2020QB074, the National Natural Science Foundation of China, Grant No. 21503056, the Fundamental Research Funds for the Central Universities. Grant No. HIT. NSRIF. 2016090. The authors gratefully acknowledge HZWTECH for providing computational facilities.

### References

- 1 Q. Zhang, J. Li, K. Shizu, S. Huang, S. Hirata, H. Miyazaki and C. Adachi, J. Am. Chem. Soc., 2012, 134, 14706-14709.
- 2 H. Uoyama, K. Goushi, K. Shizu, H. Nomura and C. Adachi, Nature, 2012, 492, 234-238.
- 3 J. Li, T. Nakagawa, J. MacDonald, Q. Zhang, H. Nomura, H. Miyazaki and C. Adachi, Adv. Mater., 2013, 25, 3319-3323.
- 4 Y. Im, M. Kim, Y. J. Cho, J. A. Seo, K. S. Yook and J. Y. Lee, Chem. Mater., 2017, 29, 1946-1963.
- 5 T. Hofbeck, U. Monkowius and H. Yersin, J. Am. Chem. Soc., 2015, 137, 399-404.
- 6 S. Hirata, Y. Sakai, K. Masui, H. Tanaka, S. Y. lee, H. Nomura, N. Nakamura, M. Yasumatsu, H. Nakanotani, Q. S. Zhang, K. Shizu, H. Miyazaki and C. Adachi, Nat. Mater., 2015, 14, 330-336.
- 7 H. T. Sun, Z. B. Hu, C. Zhong, X. K. Chen, Z. R. Sun and J.-L. Brédas, J. Phys. Chem. Lett., 2017, 8, 2393-2398.
- 8 K. Kawasumi, T. Wu, T. Y. Zhu, H. S. Chae, T. V. Voorhis, M. A. Baldo and T. M. Swager, J. Am. Chem. Soc., 2015, 137, 11908-11911.
- 9 Y. Tao, K. Yuan, T. Chen, P. Xu, H. Li, R. Chen, C. Zheng, L. Zhang and W. Huang, Adv. Mater., 2014, 26, 7931-7958.
- 10 G. Mehes, H. Nomura, Q. Zhang, T. Nakagawa and C. Adachi, Angew. Chem., Int. Ed., 2012, 51, 11311-11315.
- 11 S. Y. Lee, T. Yasuda, H. Nomura and C. Adachi, Appl. Phys. Lett., 2012, 101, 093306.
- 12 T. Nakagawa, S. Y. Ku, K. T. Wong and C. Adachi, Chem. Commun., 2012, 48, 9580-9582.
- 13 H. Nakanotani, K. Masui, J. Nishide, T. Shibata and C. Adachi, Sci. Rep., 2013, 3, 2127.
- 14 H. Tsujimoto, D.-G. Ha, G. Markopoulos, H. S. Chae, M. A. Baldo and T. M. Swager, J. Am. Chem. Soc., 2017, **139**, 4894–4900.
- 15 A. E. Nikolaenko, M. Cass, F. Bourcet, D. Mohamad and M. Roberts, Adv. Mater., 2015, 27, 7236-7240.
- 16 P. Rajamalli, N. Senthilkumar, P. Gandeepan, P. Y. Huang, M. J. Huang, C. Z. Ren-Wu, C. Y. Yang, M. J. Chiu, L. K. Chu, H. W. Lin and C. H. Cheng, J. Am. Chem. Soc., 2016, 138, 628-634.

- 17 T. Hatakeyama, K. Shiren, K. Nakajima, S. Nomura, S. Nakatsuka, K. Kinoshita, J. Ni, Y. Ono and T. Ikuta, Adv. Mater., 2016, 28, 2777-2781.
- 18 T. A. Lin, T. Chatterjee, W. L. Tsai, W. K. Lee, M. J. Wu, M. Jiao, K. C. Pan, C. L. Yi, C. L. Chung, K. T. Wong and C. C. Wu, Adv. Mater., 2016, 28, 6976–6983.
- 19 M. Numata, T. Yasuda and C. Adachi, Chem. Commun., 2015, 51, 9443-9446.
- 20 X. K. Chen, Y. Tsuchiya, Y. Ishikawa, C. Zhong, C. Adachi and J.-L. Brédas, Adv. Mater., 2017, 29, 1702767.
- 21 Q. Zhu, X. Guo and J. Zhang, J. Comput. Chem., 2019, 40, 1578-1585.
- 22 L. J. Wang, T. Li, P. C. Feng and Y. Song, Phys. Chem. Chem. Phys., 2017, 19, 21639-21647.
- 23 Y. C. Li, Z. H. Wang, X. L. Li, G. Z. Xie, D. C. Chen, Y. F. Wang, C. C. Lo, A. Lien, J. B. Peng, Y. Cao and S. J. Su, Chem. Mater., 2015, 27, 1100-1109.
- 24 X. F. Lu, S. H. Fan, J. H. Wu, X. W. Jia, Z. S. Wang and G. Zhou, J. Org. Chem., 2014, 79, 6480-6489.
- 25 P. Data, P. Pander, M. Okazaki, Y. Takeda, S. Minakata and A. P. Monkman, Angew. Chem., Int. Ed., 2016, 55, 5739-5744.
- 26 M. K. Etherington, F. Franchell, J. Gibson, T. Northey, J. Santos, J. S. Ward, H. F. Higginbotham, P. Data, A. Kurowska, P. L. D. Santos, D. R. Graves, A. S. Batsaov, F. B. Dias, M. R. Bryce, T. J. Penfold and A. P. Monkman, Nat. Commun., 2017, 8, 14987.
- 27 Z. H. Wang, Y. C. Li, X. Y. Cai, D. C. Chen, G. Z. Xie, K. K. Liu, Y. C. Wu, C. C. Lo, A. Lien, Y. Cao and S. J. Su, ACS Appl. Mater. Interfaces, 2016, 8, 8627-8636.
- 28 J. B. Im, R. Lampande, G. H. Kim, J. Y. Lee and J. H. Kwon, J. Phys. Chem. C, 2017, 121, 1305-1314.
- 29 C. C. Fan, C. B. Duan, C. M. Han, B. Han and H. Xu, ACS Appl. Mater. Interfaces, 2016, 8, 27383-27393.
- 30 C. Wang, X. L. Li, Y. Y. Pan, S. T. Zhang, L. Yao, Q. Bai, W. J. Li, P. Lu, B. Yang, S. J. Su and Y. G. Ma, ACS Appl. Mater. Interfaces, 2016, 8, 3041-3049.
- 31 S. Y. Lee, C. Adachi and T. Yasuda, Adv. Mater., 2016, 28, 4626-4631.
- 32 S. Ishijima, M. Higashi and H. Yamaguchi, J. Phys. Chem., 1994, 98, 10432-10435.
- 33 C. Ley, F. Morlet-Savary, P. Jacques and J. P. Fouassier, Chem. Phys., 2000, 255, 335-346.
- 34 A. M. Turek, G. Krishnamoorthy, K. Phipps and J. Saltiel, J. Phys. Chem. A, 2002, 106, 6044-6052.
- 35 S. Reineke and M. A. Baldo, Sci. Rep., 2014, 4, 3797.
- 36 H. Wang, L. S. Xie, Q. Peng, L. Q. Meng, Y. Wang, Y. P. Yi and P. F. Wang, Adv. Mater., 2014, 26, 5198-5204.
- 37 X. F. Wei, Y. Z. Chen, R. H. Duan, J. J. Liu, R. F. Wang, Y. W. Liu, Z. Y. Li, Y. P. Yi, Y. Y. Takamura, P. F. Wang and Y. Wang, J. Mater. Chem. C, 2017, 5, 12077-12084.
- 38 X. Wei, Z. Li, T. Hu, R. Duan, J. Liu, R. Wang, Y. Liu, X. Hu, Y. Yi, P. Wang and Y. Wang, Adv. Opt. Mater., 2019, 7, 1801767.
- 39 Y. C. Li, X. L. Li, D. J. Chen, X. Y. Cai, G. Z. Xie, Z. Z. He, Y. C. Wu, A. Lien, Y. Cao and S. J. Su, Adv. Funct. Mater., 2016, 26, 6904-6912.

**Paper** 

- 40 M. Y. Wong and E. Zysman-Colman, Adv. Mater., 2017, 29, 1605444.
- 41 Z. Tu, G. Han, T. Hu, R. Duan and Y. Yi, Chem. Mater., 2019, 31, 6665-6671.
- 42 Q. Lu, M. Qin, S. Liu, L. Lin, C.-K. Wang, J. Fan and Y. Song, Chem. Phys. Lett., 2021, 764, 138260.
- 43 Y. Liu, L. Wang, L. Xu and Y. Song, J. Mater. Chem. C, 2023, **11**, 13403-13417.
- 44 Q. Lu, G. Y. Jiang, F. Y. Li, L. L. Lin, C. K. Wang, J. Z. Fan and Y. Z. Song, Spectrochim. Acta, Part A, 2020, 229, 117964.
- 45 Q. Peng, D. Fan, R. H. Duan, Y. P. Yi, Y. L. Niu, D. Wang and Z. G. Shuai, J. Phys. Chem. C, 2017, 121, 13448-13456.
- 46 Q. Peng, Y. L. Niu, Q. Shi, X. Gao and Z. G. Shuai, J. Chem. Theory Comput., 2013, 9, 1132-1143.
- 47 Y. L. Niu, O. Peng, C. M. Deng, X. Gao and Z. G. Shuai, J. Phys. Chem. A, 2010, 114, 7817-7831.
- 48 B. Miehlich, A. Savin, H. Stoll and H. Preuss, Chem. Phys. Lett., 1989, 157, 200-206.
- 49 C. Adamo and V. Barone, Toward Reliable Density Functional Methods without Adjustable Parameters: The PBE0 Model, J. Chem. Phys., 1999, 110, 6158-6170.
- 50 C. A. Guido, E. Bremond, C. Adamo and P. Cortona, J. Chem. Phys., 2013, 138, 021104.
- 51 A. D. Boese and J. M. L. Martin, J. Chem. Phys., 2004, 121, 3405-3416.
- 52 Y. Zhao and D. G. Truhlar, Theor. Chem. Acc., 2008, 120, 215-241.
- 53 T. Yanai, D. P. Tew and N. C. Handy, Chem. Phys. Lett., 2004, 393, 51-57.
- 54 Y.-S. Lin, G.-D. Li, S.-P. Mao and J.-D. Chai, J. Chem. Theory Comput., 2013, 9, 263-272.
- 55 H. Ma, W. Shi, J. Ren, W. Li, Q. Peng and Z. Shuai, J. Phys. Chem. Lett., 2016, 7, 2893-2898.
- 56 J. Liu, J. Fan, K. Zhang, Y. Zhang, C.-K. Wang and L. Lin, Chin. Phys. B, 2020, 29, 088504.
- 57 Q. Peng, Y. Yi, Z. Shuai and J. Shao, J. Chem. Phys., 2007, 126, 114302.
- 58 J. Tomasi, B. Mennucci and R. Cammi, J. Cheminform., 2005, **105**, 2999-3093.
- 59 M. J. Frisch, G. W. Trucks, H. B. Schlegel, G. E. Scuseria, M. A. Robb, J. R. Cheeseman, G. Scalmani, V. Barone, B. Mennucci, G. A. Petersson, H. Nakatsuji, M. Caricato, X. Li, H. P. Hratchian, A. F. Izmaylov, J. Bloino, G. Zheng, J. L. Sonnenberg, M. Hada, M. Ehara, K. Toyota, R. Fukuda, J. Hasegawa, M. Ishida, T. Nakajima, Y. Honda, O. Kitao, H. Nakai, T. Vreven, J. A. Montgomery Jr, J. E. Peralta, F. Ogliaro, M. Bearpark, J. J. Heyd, E. Brothers, K. N. Kudin, V. N. Staroverov, R. Kobayashi, J. Normand, K. Raghavachari, A. Rendell, J. C. Burant, S. S. Iyengar, J. Tomasi, M. Cossi, N. Rega, J. M. Millam, M. Klene,

- J. E. Knox, J. B. Cross, V. Bakken, C. Adamo, J. Jaramillo, R. Gomperts, R. E. Stratmann, O. Yazyev, A. J. Austin, R. Cammi, C. Pomelli, J. W. Ochterski, R. L. Martin, K. Morokuma, V. G. Zakrzewski, G. A. Voth, P. Salvador, J. J. Dannenberg, S. Dapprich, A. D. Daniels, Ö. Farkas, J. B. Foresman, J. V. Ortiz, J. Cioslowski and D. J. Fox, Gaussian 09, Revision D.01, Gaussian Inc., Wallingford, CT, 2010.
- 60 Y. L. Niu, W. Q. Li, Q. Peng, H. Geng, Y. P. Yi, L. J. Wang, G. J. Nan, D. Wang and Z. G. Shuai, Mol. Phys., 2018, 116, 1078-1090.
- 61 Q. Peng, Y. P. Yi, Z. G. Shuai and J. S. Shao, J. Am. Chem. Soc., 2007, 129, 9333-9339.
- 62 Y. L. Niu, Q. Peng and Z. G. Shuai, Sci. China Ser. B-Chem., 2008, 51, 1153-1158.
- 63 Z. G. Shuai, Chin. J. Chem., 2020, 38, 1223-1232.
- 64 Z. G. Shuai and Q. Peng, Phys. Rep., 2014, 537, 123-156.
- 65 Z. G. Shuai and Q. Peng, Nat. Sci. Rev., 2017, 4, 224-239.
- 66 DALTON. A molecular electronic structure program, Release Dalton 2019. Alpha, 2019, https://daltonprogram.org/.
- 67 K. Aidas, C. Angeli, K. L. Bak, V. Bakken, R. Bast, L. Boman, O. Christiansen, R. Cimiraglia, S. Coriani, P. Dahle, E. K. Dalskov, U. Ekström, T. Enevoldsen, J. J. Eriksen, P. Ettenhuber, B. Fernández, L. Ferrighi, H. Fliegl, L. Frediani, K. Hald, A. Halkier, C. Hättig, H. Heiberg, T. Helgaker, A. C. Hennum, H. Hettema, E. Hjertenæs, Høst, I.-M. Høyvik, M. F. Iozzi, B. Jansik, H. J. A. Jensen, D. Jonsson, P. Jørgensen, J. Kauczor, Kirpekar, T. Kjærgaard, W. Klopper, S. Knecht, Kobayashi, H. Koch, J. Kongsted, A. Krapp, R. K. Kristensen, A. Ligabue, O. B. Lutnæs, J. I. Melo, K. V. Mikkelsen, R. H. Myhre, C. Neiss, C. B. Nielsen, P. Norman, J. Olsen, J. M. H. Olsen, A. Osted, M. J. Packer, F. Pawlowski, T. B. Pedersen, P. F. Provasi, S. Reine, Z. Rinkevicius, T. A. Ruden, K. Ruud, V. Rybkin, P. Salek, C. C. M. Samson, A. Sánchez de Merás, T. Saue, S. P. A. Sauer, B. Schimmelpfennig, K. Sneskov, A. H. Steindal, K. O. Sylvester-Hvid, P. R. Taylor, A. M. Teale, E. I. Tellgren, D. P. Tew, A. J. Thorvaldsen, L. Thøgersen, O. Vahtras, M. A. Watson, D. J. D. Wilson, M. Ziolkowski and H. Ågren, Wiley Interdiscip. Rev.: Comput. Mol. Sci., 2014, 4, 269-284.
- 68 T. Lu and F. W. Chen, J. Comput. Chem., 2012, 33, 580-592.
- 69 Z. Y. Liu, T. Lu and Q. X. Chen, Carbon, 2020, 165, 461-467.
- 70 J. Leng, Z. Zhang, Y. Zhang, J. Sun and H. Ma, J. Lumin., 2018, 204, 312-318.
- 71 J. Fan, L. Cai, L. Lin and C.-K. Wang, Phys. Chem. Chem. Phys., 2017, 19, 29872-29879.
- 72 B. Liu, H. Nie, X. Zhou, S. Hu, D. Luo, D. Gao, J. Zou, M. Xu, L. Wang, Z. Zhao, A. Qin, J. Peng, H. Ning, Y. Cao and B. Z. Tang, Adv. Funct. Mater., 2016, 26, 776–783.